PRELIMINARY MODELING OF ROCK WETTABILITY ALTERATION DURING LOW-SALINITY WATERFLOODING USING TOUGH2–TMGAS

Marica Marcolini[(1)], Franco Masserano[(2)], Alfredo Battistelli[(1)]

(1) RISAMB Dept., Environmental Engineering Unit, Saipem SpA (Eni Group), 61032 Fano (PU), Italy
(2) TEOR Dept., E&P Division, Eni SpA, 20097 San Donato Milanese (MI), Italy
e-mail: marica.marcolini@saipem.eni.it, franco.masserano@eni.it, alfredo.battistelli@saipem.eni.it

ABSTRACT

Laboratory experiments and field tests suggest that under proper conditions, the injection of low-salinity water (instead of high-salinity brine) may improve oil recovery during waterflooding. Even though the exact EOR mechanisms are not fully understood, the change of rock wettability from Oil-Wet (OW) or Mixed-Wet (MW) towards Water-Wet (WW) conditions has been invoked to explain the increased oil recovery with low salinity waterflooding. From a modeling point of view, the wettability alteration has been tentatively described by a change from oil-wet to water-wet relative characteristic curves linked to the local salt content of the aqueous phase.

Within a R&D project aimed to investigate low-salinity waterflooding as an improved oil recovery method, the advanced modeling capabilities required to simulate the involved processes have been coded into the TMGAS EOS module of TOUGH2 reservoir simulator. The new features include (i) the treatment of OW and MW domains in addition to the WW conditions conventionally assumed by TOUGH2; (ii) the switching from OW or MW to WW relative permeability and capillary pressure curves, depending on the local sodium chloride concentration.

INTRODUCTION

Waterflooding is the most widely applied technique to sustain oil production affected by reservoir pressure depletion. It allows pressure maintenance and oil displacement towards the production wells. Enhanced Oil Recovery (EOR) processes involve the injection of fluids into the reservoir, whereupon the injected fluid interacts with the reservoir rock/oil system to create conditions favorable for oil recovery (Green and Willhite, 1998). The main physical and chemical mechanisms leading to an improvement in oil displacement efficiency can act throughout oil viscosity reduction, oil swelling, mass transfer between oil and solvent, interfacial tension (IFT) reduction, wettability modifications, or favorable phase behavior.

Low-salinity waterflooding is an EOR method presently under evaluation, consisting of the injection of low-salinity brine to improve oil recovery over conventional higher salinity waterflooding. The availability and the assurance that it does not affect formation injectivity are traditionally the main factors affecting the choice of the waterflooding brine. Less attention has been placed so far on how brine composition affects displacement efficiency. Laboratory experiments indicate that injection of low-salinity brine can provide a marked increase in oil recovery (Tang and Morrow, 1997, 1999; Webb et al., 2004, 2005; McGuire et al., 2005; Zhang and Morrow, 2006; Lager et al., 2006, 2008) compared to injection of seawater or high-salinity produced water. Due to the complexity of the crude oil/brine/rock interactions, discussion of the mechanisms by which oil recovery is improved due to low-salinity waterflooding is still open. The formulated hypotheses include increasing pH leading to *in situ* saponification and IFT reduction, emulsion formation, clay migration, multi-component ion exchange (MIE), and wettability alterations.

Regardless of the mechanism, the reservoir rock and fluids need to satisfy certain requirements for low-salinity waterflooding to be successful (Jerauld et al, 2006): connate water must be present, reservoir oil must contain polar components, and reservoir rock must contain minerals with cation exchange capacity as clay minerals (Lager et al., 2006). Most of the proposed theories that explain the increase in oil recovery with a change in injected brine salinity are consistent with the results of Tang and Morrow (1997). They suggest that the complexity of oil-brine-reservoir interactions controls the wettability by a variety of possible mechanisms and, moreover, that changes from OW or MW conditions toward WW occur with a decrease in salinity, together with oil recovery by spontaneous imbibition and oil recovery by waterflooding.

THE TOUGH2-TMGAS SIMULATOR

TMGAS (Battistelli and Marcolini, 2009) is an EOS module specifically designed for the TOUGH2 reservoir simulator (Pruess et al., 1999), able to model the two-phase flow of an aqueous (Aq) and a nonaqueous (NA) phase in deep geological structures. TMGAS can simulate the two-phase behavior of NaCl-dominated brines in equilibrium with a NA mixture containing hydrocarbons (pure as well as pseudo-components) and inorganic gases. The

NA phase can be either in gas, supercritical, or liquid (condensed) conditions, with the limitation that such conditions cannot coexist within the same grid element. The PR cubic EOS (Peng and Robinson, 1976), with the modifications suggested by Soreide and Whitson (1992), is used for phase-equilibria calculations.

NA phase density is computed using the PR EOS, accounting for conventional volume shift correction, whereas departure enthalpy and dynamic viscosity are computed using the LK EOS (Lee and Kesler, 1975) and the Friction Theory Model (Quinones-Cisneros et al., 2001), respectively. The most accurate Friction Theory Model with seven adjustable parameters was calibrated for all the pure components covered by the internal database of TMGAS against the NIST Web Database REFPROP7 (Lemmon et al., 2002). In addition, the general one-parameter Friction Theory Model is available in the code, specifically implemented for pseudo-components and species not already supported by the internal database. This can be very useful when dealing with ordinary petroleum mixtures generally described by means of both pure components and pseudo-components. Brine properties are evaluated using updated versions of the correlations implemented in the EWASG EOS module (Battistelli et al., 1997) for water and sodium chloride mixtures. For a detailed description of TMGAS, refer to Battistelli and Marcolini (2009).

WETTABILITY ALTERATION MODEL

A model was developed to describe the wettability alteration from OW or MW conditions to WW, consequent to the low-salinity brine injection into the reservoir. The model is inspired by the work of Delshad et al. (2006) for the reservoir simulator UTCHEM (University of Texas, 2000) concerning rock wettability changes induced by the injection of an aqueous solution containing a specific polymer. It is based on the introduction of two sets of relative permeability and capillary pressure curves corresponding to the "initial" wettability conditions (OW or MW) and final wettability conditions (WW). The property value is obtained by linear interpolation between initial and final conditions:

$$k_{r_\beta} = \omega\, k_{r_\beta}^{initial} + (1-\omega)\, k_{r_\beta}^{final} \qquad (1)$$

$$P_c = \omega\, P_c^{initial} + (1-\omega) P_c^{final} \qquad (2)$$

where $k_{r\beta}$ indicates the relative permeability to the phase β and P_c is the capillary pressure. The interpolation parameter ω is correlated to the normalized concentration of salt in the two component water–sodium chloride system, as given by Equation (3), where X indicates the mass fraction in the Aq phase.

$$X_{Aq}^{\overline{NaCl}} = \frac{X_{Aq}^{NaCl}}{X_{Aq}^{NaCl} + X_{Aq}^{H_2O}} \qquad (3)$$

Analogously to Jerauld et al. (2006), two threshold values for the normalized sodium chloride concentration, $X_{\max}^{wet}$ and $X_{\min}^{wet}$, are assumed. During the dilution process, when the normalized NaCl mass fraction reaches the upper bound, the transition from initial to final wettability conditions begins. Until the salt concentration is comprised between the two concentration thresholds, relative permeabilities and capillary pressure are calculated as indicated by Equations (1) and (2). The wettability alteration process toward WW conditions is completed when the salt concentration becomes lower than the lower threshold value.

The proposed modeling approach requires that the interpolation parameter ω assumes the following values outside the interpolation interval:

$$\omega = 1 \quad \text{if} \quad X_{Aq}^{\overline{NaCl}} \geq X_{\max}^{wet} \qquad (4)$$

$$\omega = 0 \quad \text{if} \quad X_{Aq}^{\overline{NaCl}} \leq X_{\min}^{wet} \qquad (5)$$

For intermediate sodium chloride concentrations, a specific interpolation function is needed. TOUGH2-TMGAS implements three different formulations, based on linear and trigonometric functions.

TOUGH2 assumes the porous medium is always under WW conditions; since the NA phase pressure is the reference pressure, the capillary pressure is always negative. This limitation is removed in order to implement the wettability alteration model by introducing the wettability index IOW, defined for each gridblock. IOW assumes the following values:

- 0 in WW conditions (default)
- 1 in OW conditions
- 2 in MW conditions

In the present formulation, wettability conditions other than WW are available only by selecting the Corey characteristic curves for phase relative permeability and capillary pressure. The Corey model for strongly WW or strongly OW conditions is defined as follows:

$$k_{r_\beta} = k_{r_\beta}^{o}\, S_{n_\beta}^{E_\beta} \qquad (6)$$

$$P_c = C_{Pc} \sqrt{\frac{\Phi}{k}} \left(1 - S_{n_\beta}\right)^{E_{Pc}} \qquad (7)$$

where Φ and k are porosity and absolute permeability, respectively; the relative permeability end point $k_{r_\beta}^{o}$ and the exponent E_β depend on phase β, and C_{Pc} and E_{Pc} are constants. To satisfy the TOUGH2 convention, C_{Pc} is negative for WW

conditions and positive for OW conditions. The normalized saturation $S_{n\beta}$ is given by:

$$S_{n\beta} = \min\left[1, \max\left(0, \frac{S_\beta - S_{\beta_r}}{1 - S_{wr} - S_{or}}\right)\right] \quad (8)$$

For a MW porous medium, Corey's model for relative permeability is unchanged, whereas the capillary pressure needs substantial variations. The curve is subdivided into a positive and negative branch, and the capillary pressure cancels out if the Aq phase saturation is equal to a specific S^*. If $S_w \le S^*$:

$$S_{nw} = \min\left[1, \max\left(0, \frac{S^* - S_w}{S^* - S_{wr}}\right)\right] \quad (9)$$

$$P_{cw} = C_{Pcw}\sqrt{\frac{\Phi}{k}} S_{nw}{}^{e_{Pcw}} \quad (10)$$

while if $S_w \ge S^*$:

$$S_{no} = \min\left[1, \max\left(0, \frac{S_w - S^*}{1 - S_{or} - S^*}\right)\right] \quad (11)$$

$$P_{co} = C_{Pco}\sqrt{\frac{\Phi}{k}} S_{no}{}^{e_{Pco}} \quad (12)$$

New necessary parameters are supplied throughout the ROCKS and SELEC data blocks. The estimation of the interpolation parameter ω is performed in the two-phase section of the EOS module. Regardless of the salt concentration, WW conditions cannot be changed and ω is set at zero. Only if IOW is not equal to zero, then ω assumes a unit value or is calculated on the basis of previously introduced functional forms.

1D LINEAR SIMULATIONS

The constant injection rate of low-salinity brine in a homogeneous and isotropic reservoir of 1000 m length is modeled using a 1D Cartesian grid. The system is discretized into 100 elements of 10 m length and constant cross area of 100 m^2. The system is initially in OW conditions and at residual saturation of the aqueous phase. Brine is injected on one side of the grid while, on the opposite side, constant conditions equal to initial conditions are maintained. The salinity of the injected brine is lower than the salinity of the reservoir connate brine and low enough to start a rock wettability alteration process. The upper threshold value of normalized sodium chloride concentrations is set equal to 10,000 ppm, while the lower threshold limit is set equal to 2000 ppm. The sinusoidal functional form for the interpolation parameter ω was adopted for every simulation. The main petrophysical properties of the reservoir and thermophysical parameters of fluid phases are listed in Table 1. Except for a negligible amount of water imposed by the two-phase equilibrium with the Aq phase, it is assumed that the NA phase is composed of just one component, described by means of the pseudo-component approach. The Friction Theory Model and the Peneloux volume shift have been used to reproduce, respectively, the oil viscosity and density specified in Table 1. The parameters of the relative permeability and capillary pressure curves specific of initial OW and final WW conditions are listed In Table 2.

Table 1. Main petrophysical properties of the reservoir and thermophysical properties of the fluid phases.

Initial pressure (Pa)	100×10^5
Constant temperature (°C)	40
Initial salinity (molal)	0.9
Absolute permeability (m^2)	5.0×10^{-12}
Porosity	0.20
Initial brine density (kg/m^3)	997.25
Initial oil density (kg/m^3)	637.35
Initial brine viscosity (Pa s)	0.6550×10^{-3}
Initial oil viscosity (Pa s)	4.4856×10^{-3}
Brine injection rate ($kg/s)/m^2$	1.002E-2
Mobility ratio[1] (OW)	11.98
Mobility ratio (WW)	2.74

Table 2. Parameters of initial (OW) and final (WW) relative permeability and capillary pressure curves.

	Oil-Wet	***Water-Wet***
Swr	0.35	0.40
Sor	0.35	0.10
Krw,0	0.7	0.4
Kro,0	0.4	1
Ekw	2	2
Eko	2	2
Cpc	0.51371	-0.51371
Epc	6.2	4

Continuous injection of low-salinity brine

An aqueous solution with NaCl concentration of 1000 ppm is injected for 1 year. Relative permeability and capillary pressure evolution in a grid element close to the boundary opposite to the injection is shown in Figure 2. Figure 1 and 2 show that, initially, both relative permeabilities and capillary pressure follow the OW characteristic curves. When the concentration in the gridblock

[1] Mobility ratio definition by Green and Willhite (1998):

$$M = \left(\frac{k_{rw}}{\mu_w}\right)_{S_{or}} \left(\frac{\mu_o}{k_{ro}}\right)_{S_{wr}}$$

reaches the upper salinity limit, the linear interpolation process between OW and WW curves starts and continues until the lower salinity threshold is achieved. From that point on, the WW characteristic curves are maintained.

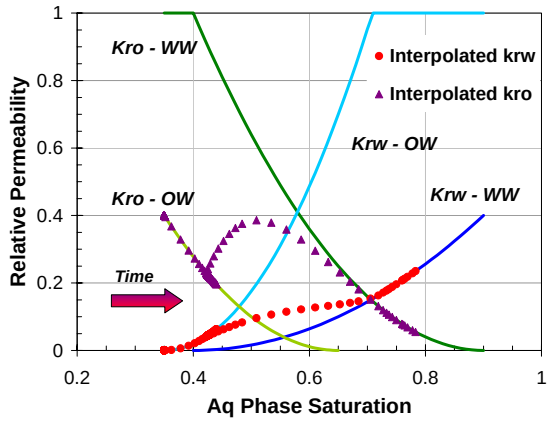

Figure 1. OW and WW relative permeabilities as functions of Aq phase saturation and calculated relative permeabilities at the end of the 1D grid as time increases.

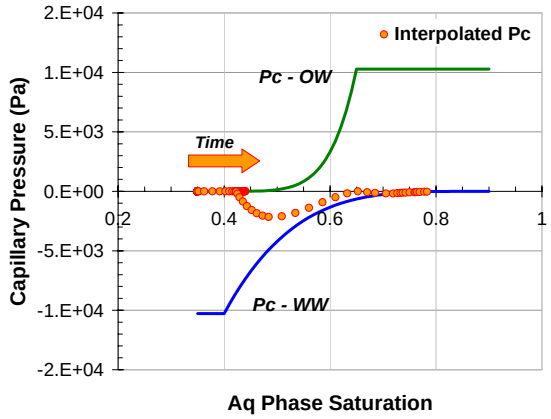

Figure 2. OW and WW capillary pressures as functions of Aq phase saturation and calculated capillary pressure in an observation grid element as time increases.

Figure 3 shows, at fixed simulation times, the profiles of Aq phase saturation and NaCl mass fraction as a function of the distance from the injection well. The injected brine displaces the reservoir oil, so the Aq phase saturation increases with time, whereas the Aq phase salinity decreases. As shown in Figure 5, after 1 month of injection, the final WW conditions have been established only in the first few gridblocks. However, after 9 months, the salt concentration drops below the lower boundary of 2000 ppm over the entire system, and the rock domain becomes completely WW.

As can be seen in Figure 3, at great distances the Aq phase saturation takes on a value slightly greater than the residual brine saturation. This is due to the formation of a "connate water bank" more evident in Figure 5 relative to a fairly short simulation time of 1.5×10^6 s. Initially the injected brine displaces the connate brine that accumulates ahead of the oil displacement front, denoted by a vertical dotted line for both low- and high-salinity injection cases. As time increases, in a growing number of grid elements, the wettability alteration process toward WW conditions takes place: oil phase mobility increases, together with the volume accessible to the aqueous phase. In Figure 5, the distance covered by the final WW conditions is highlighted by a vertical black dotted line.

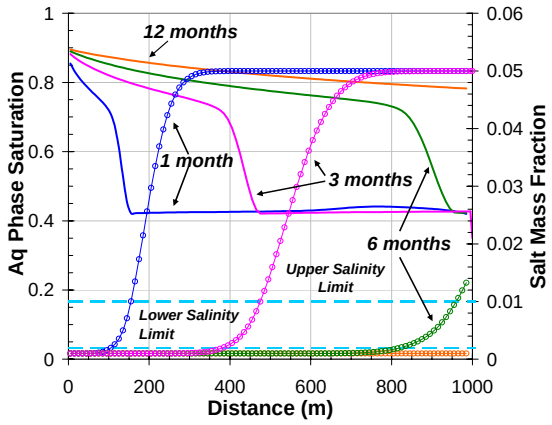

Figure 3. Continuous injection of low salinity brine: Aq phase saturation (continuous line) and NaCl concentration (line plus symbols) at four different times.

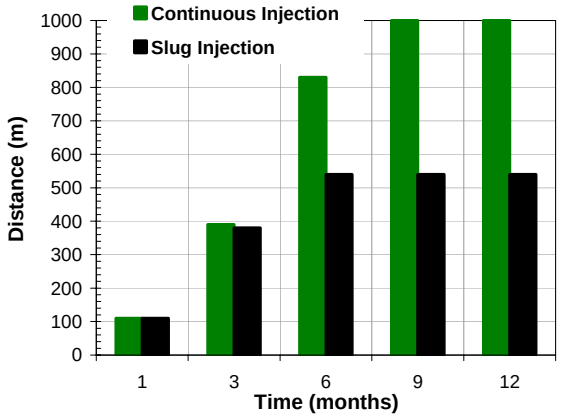

Figure 4. Continuous injection of low salinity brine vs. slug injection: location of wettability change front from OW to WW conditions at fixed simulation times.

Slug injection of low salinity brine

If low-salinity brine must be provided by treating higher salinity brines, it could be more convenient to inject limited amounts of low-salinity brine, followed by the conventional waterflooding process.

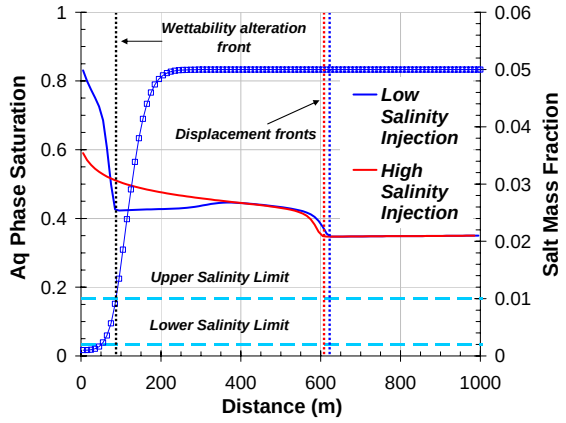

Figure 5. Comparison between Aq phase saturation profiles (continuous line) resulting from high and low salinity injection and NaCl concentration profile (line plus symbol) at a short time (t=17.36 days).

Leaving the same total simulation time, first we inject low-salinity brine for two months and brine with the same connate brine composition for the residual time (referred to from here on as "high salinity brine"). As shown in Figure 4, after 6 months the wettability alteration process is completely arrested, and water wet conditions have been established in the first 520 m of the system. Oil mobilized in these gridblocks accumulates downstream, generating an "oil bank" (Figure 6) that is slowly displaced as time increases.

The NaCl concentration profiles reported in Figure 7 show that high-salinity injection interrupts dilution. The salt mass fraction again rises over the upper salinity threshold, limiting the wettability alteration process to a small region of the system.

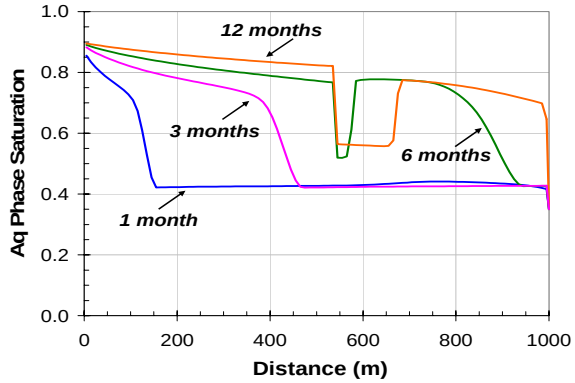

Figure 6. Slug injection of low salinity brine: Aq phase saturation profiles at four different times.

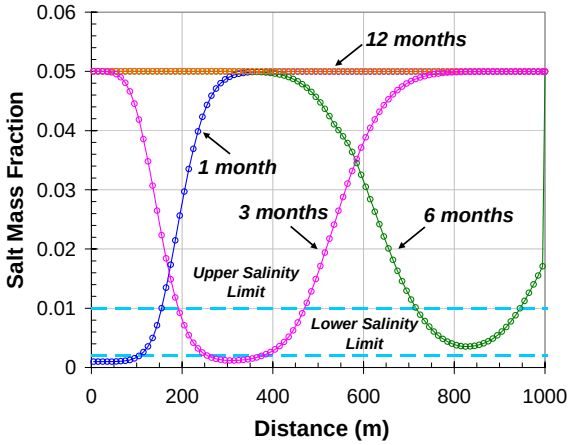

Figure 7. Slug injection of low salinity brine: NaCl concentration profiles at four different times.

In Figure 8, the cumulative oil recovery relative to the previously described cases can be analyzed, together with the upper and lower bounds of achievable oil recovery, represented by the waterflooding in a WW domain (independent on brine salinity) and by the injection of the high salinity brine, respectively. All simulations are performed at the same initial conditions. Then, if the rock-domain is WW, the aqueous phase saturation of 0.35 is less than the WW irreducible water saturation equal to 0.40. Fig. 8 shows that the change in slope indicative of the water breakthrough is delayed for a WW domain, due to the higher AQ phase irreducible saturation of the WW domain compared to the cases characterized by an initial OW domain. In the three examined OW scenarios the aqueous phase breakthrough takes place at the same injection time since it occurs so rapidly as to anticipate the beginning of wettability alteration process.

The oil recovery factor is strongly affected by the residual oil saturation specific of the final wettability status reached in the reservoir. In general, compared with an OW domain, a WW domain is characterized by lower residual oil saturation since it tends to retain water. Regardless of the speed, the maximum achievable oil recovery is that obtainable if WW conditions are established in all grid-block elements. On the other hand, if OW conditions persist all over the system the oil recovery is minimum. While intermediate amounts of produced oil correspond to those situations wherein the wettability alteration process is completed only in a section of the total domain.

Concerning the two cases described above, the continuous injection of low-salinity brine seems to add minor increments to the recovery factor compared to the 2 months of slug injection.

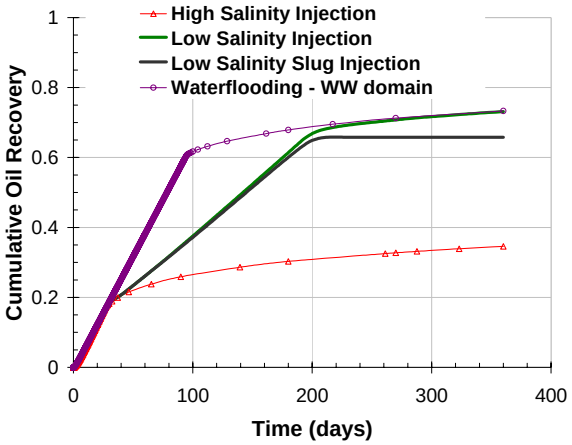

Figure 8. Comparison among the cumulative oil recovery obtained with waterflooding of a WW domain and an OW domain with high salinity brine and with continuous and slug low salinity injection.

5-SPOT WELL PATTERN SIMULATIONS

The slug injection of low-salinity brine is also modeled by using a 5-spot well pattern approach. The 2D Cartesian grid was generated with the PATTY code (Fuller e Pruess, 1985) developed at LBNL for simulators of the TOUGH2 family. Since simulation results can be affected by grid orientation effects, a 9-point differencing scheme was adopted with a parallel grid. Due to the symmetry of the system, the simulations are limited to 1/8 sector of a 5-spot well pattern. The horizontal layer is discretized into 121 elements, for a total surface area of 20,240 m^2, with the injector-producer spacing equal to 284.5 m. The parameters of relative permeabilities and capillary pressure curves specific for initial OW and final WW conditions are in Table 3.

Table 3. Parameters of initial (OW) and final (WW) relative permeability and capillary pressure curves.

	Oil-Wet	***Water-Wet***
Swr	0.15	0.20
Sor	0.35	0.20
Krw,0	0.6	0.2
Kro,0	0.4	1
Ekw	2	5
Eko	6	2
Cpc	0.7	-0.7
Epc	3	3

Both the continuous (Case A) and the 0.25 PV slug (Case B) injection of low-salinity brine have been simulated. The system initially has a brine phase at irreducible saturation with a 0.9 molal NaCl concentration. Initial pressure and temperature are, respectively, 136.2 bar abs and 39.44°C. Porosity, absolute permeability, oil properties, and the wettability alteration model used for the 1D simulation have been preserved. Brine is injected at a constant rate of 0.0255 $kg \cdot s^{-1} \cdot m^{-1}$, and production occurs with a well on deliverability at a constant bottomhole pressure of 130 bar abs.

Figure 9 shows the Aq phase saturation and NaCl mass fraction profiles in the production well block for both cases A and B. Since oil displacement occurs preferentially along the connection between injection and production wells, the Aq phase breakthrough takes place just after 0.15 injected PV, as attested by the early increment of the Aq phase saturation.

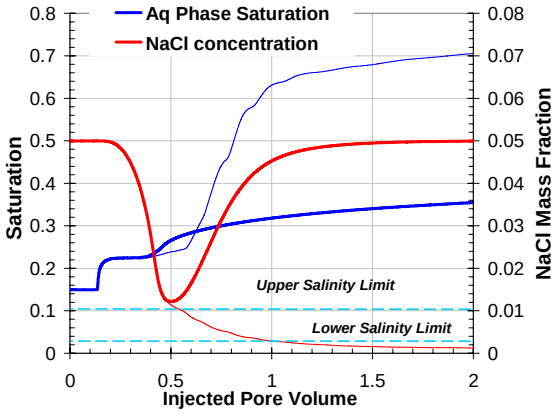

Figure 9. Case A (thin line) and B (thick line): Aq phase saturation and NaCl concentration as function of injected PV.

The Aq phase saturation remains stable until the transit of the connate water bank is completed, and then it starts increasing again while the wettability alteration process advances toward WW conditions. Figures 10 and 11 show the NA-phase saturation distribution for cases A and B, respectively, corresponding to four subsequent simulation times.

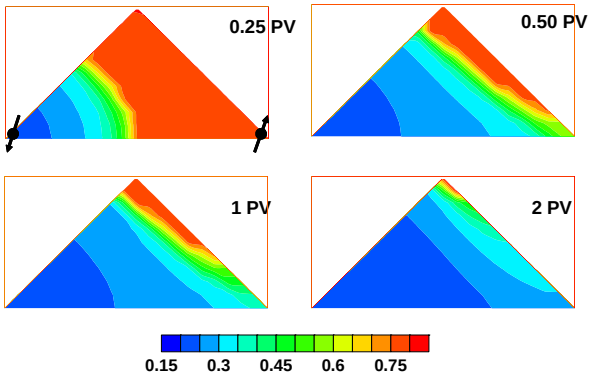

Figure 10. Case A: NA phase saturation distribution at different injected pore volumes.

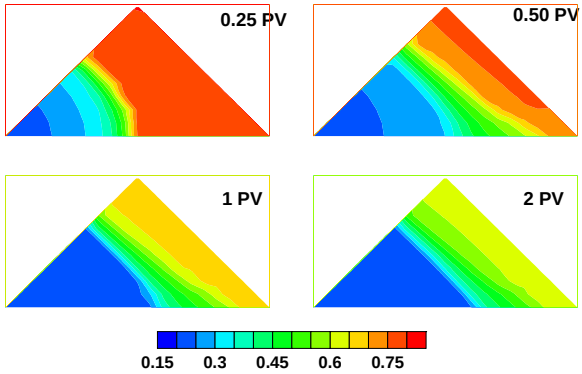

Figure 11. Case B: NA phase saturation distribution at different injected pore volumes.

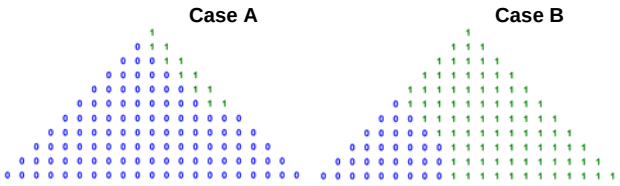

Figure 12. Case A and B: WW conditions distribution at final simulation time (0= WW, 1=OW).

At final simulation time, Case A oil saturation is close to the WW residual saturation almost everywhere over the domain, while in the other scenario, the preservation of OW conditions in a large number of the gridblocks (Figure 12) prevents an increase in oil-phase mobility.

The NaCl concentration evolution is shown in Figures 13 and 14. Moving away from the injection well, the low-salinity slug mixes with the connate brine, while the high-salinity brine injected upstream and the resulting NaCl concentration do not favor a consistent WW-condition advancement. At final simulation time, the initial salt mass fraction is almost fully restored over the entire domain.

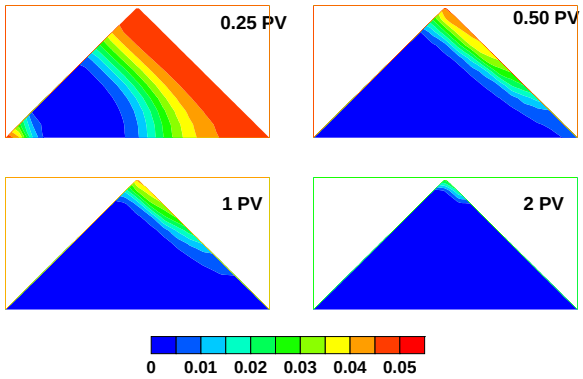

Figure 13. Case A: NaCl mass fractions distribution at different injected pore volumes.

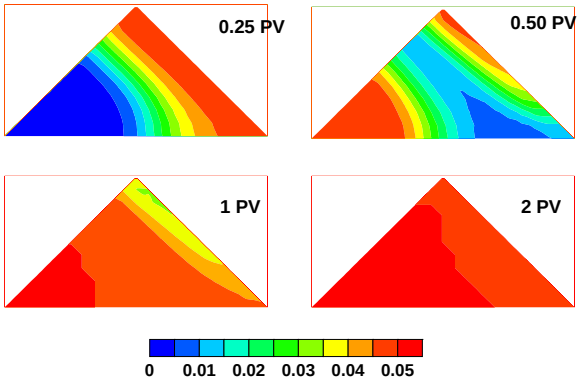

Figure 14. Case B: NaCl mass fraction distribution at different injected pore volumes.

Figure 15 shows a comparison between the oil recovery curves in the two considered scenarios. In Case A, the final oil recovery is ~70% of the Original Oil In Place (OOIP), while it decreases to 50% if only a low-salinity brine slug is injected—it is strongly dependent on the advancement of the WW-conditions front and, then, on slug size. Note that a 20% increment of oil recovery requires injecting a low-salinity volume eight times that of the slug.

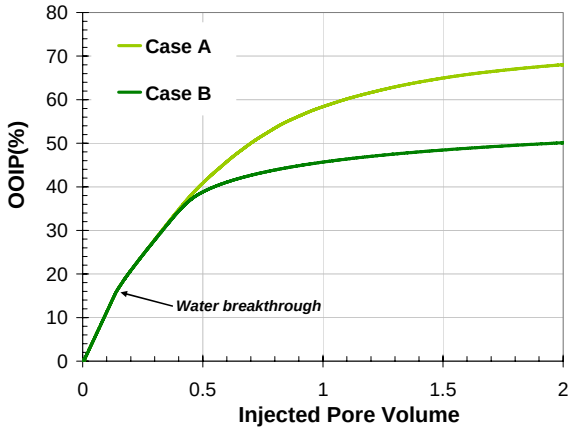

Figure 15. Case A and B: OOIP(%) as function of injected pore volumes.

CONCLUSIONS

Although experimental results and field tests seem to confirm the effectiveness of low-salinity waterflooding, the exact mechanisms responsible for the oil recovery increase are still to be understood. Among the modeling solutions proposed to simulate the observed EOR phenomena by Jerauld et al. (2006), the most important is the alteration of rock wettability conditions as a function of Aq phase salinity in the reservoir.

The effects of salt concentration on relative permeability and capillary pressure characteristic curves were treated with a simplified approach, similar to that used by Delshad et al. (2006) concerning the

wettability alteration induced by surfactant and/or polymer injection. The formulated model consists substantially in the introduction of two sets of characteristic curves, specific of initial (OW or MW) and final (WW) rock wettability conditions. The relative permeability and capillary pressure values are the result of linear interpolations depending on parameter ω, strongly correlated to the local salt concentration. Parameter ω can vary from 1 to 0 according to different functional forms. The model was implemented in the TMGAS EOS module (Battistelli and Marcolini, 2009) of the TOUGH2 reservoir simulator (Pruess et al., 1999).

To verify the performances of the wettability alteration model and analyze related processes during waterflooding, different simulations have been presented. A 1D Cartesian grid and a 2D 5-spot well pattern have been used. Both continuous and slug injection of low-salinity brine have been simulated, evaluating the additional reservoir oil recovery of low-salinity injection compared with the high-salinity injection. The formation of a connate water bank, as described in Jerauld et al. (2006), has been observed. Numerical simulation seems to be a promising tool for analyzing laboratory and field tests and optimizing low salinity waterflooding operations.

ACKNOWLEDGMENTS

This work was performed within the EFIP R&D project sponsored and coordinated by the Eni E&P Division. The authors would like to thank the E&P Division for permission to publish this paper.

REFERENCES

Battistelli A. and M. Marcolini, TMGAS: a new TOUGH2 EOS module for the numerical simulation of gas mixtures injection in geological structures, *Intl. J. Greenhouse Gas Control*, 3, 481-493, 2009.

Battistelli A., Calore C. and K. Pruess, The simulator TOUGH2/EWASG for modelling geothermal reservoirs with brines and a non-condensible gas. *Geothermics*, 26, 4,437-464, 1997.

Corey A. T., The interrelation between gas and oil relative permeabilities. *Producers Monthly*, 38-41, November, 1954.

Delshad M., Najafabadi N.F., Anderson G.A, Pope G.A. and K. Sepehrnoori, Modeling Wettability Alteration in Naturally Fractured Reservoirs. SPE 100081 Paper presented at SPE/DOE Symposium on Improved Oil Recovery held in Tulsa, Oklahoma, U.S.A, 22-26 April, 2006.

Fuller P. and K. Pruess, PATTY – A mesh generator for simulations of five-, seven-, and nine-spot floods, Report LBNL-20739, Lawrence Berkeley National Laboratory, Berkeley, Calif., 1985.

Green D.W. and G.P. Willhite, *Enhanced Oil Recovery*, Henry L. Doherty Memorial Fund of AIME, Society of Petroleum Engineers, Richardson, Texas, 1998.

Jerauld G.R., Lin C.Y., Webb K.J. and J.C. Seccombe, Modeling low-salinity waterflooding. SPE 102239, 2006.

Lager A., Webb K.J., Black C.J.J., Singleton M. and K.S. Sorbie, Low salinity oil recovery – An experimental investigation. Paper SCA 2006-36 (Intl. Symp. Society of Core Analysts), 2006.

Lager A., Webb K.J., Collins I.R. and D.M. Richmond, LoSal™ Enhanced Oil Recovery: Evidence of Enhanced Oil Recovery at the Reservoir Scale, SPE 113976, 2008.

Lee B.I. and M.G. Kesler, A generalized thermodynamic correlation based on three-parameter corresponding states, *AICHE J.*, 21, 3, 510-527, 1975.

Lemmon E.W., McLinden M.O., Huber M.L., *Reference Fluid Thermodynamic and Transport Properties*, NIST Standard Reference Database 23, Version 7.0, 2002.

McGuire P.L., Chatam J.R., Paskvan F.K., Sommer D.M. and F.H. Carini, Low salinity oil recovery: an exciting opportunity for Alaska's North Slope. SPE 93903, Western Regional Meeting, Irvin, CA, 30 March-1 April, 2005.

Peng D.Y. and D.B. Robinson, A New Two-Constant Equation of State. *Ind. Eng. Chem. Fund.* 15, 59-64, 1976.

Pruess K., C. Oldenburg, and G. Moridis, *TOUGH2 User's Guide, Version 2.0*, Report LBNL-43134, Lawrence Berkeley National Laboratory, Berkeley, CA, 1999.

Soreide I. and C.H. Whitson, Peng-Robinson predictions for hydrocarbons, CO_2, N_2, and H_2S with pure water and NaCl brine, *Fluid Phase Equilibria,* 77, 217-240, 1992.

Tang G.Q. and N.R. Morrow, Salinity, temperature, oil composition, and oil recovery by waterflooding, *SPE Reservoir Engineering* 33680, 1997.

Tang G.Q. and N.R. Morrow, Influence of brine composition and fines migration on crude oil/brine/rock interactions and oil recovery. *J. of Petroleum Science and Eng.*, 24, 99-111, 1999.

University of Texas, *User's Guide for UTCHEM-9.0: A Three-dimensional Chemical Flood Simulator.* Reservoir Engineering Research Program Center for Petroleum and Geosystems Engineering, The University of Texas at Austin, Texas, 78712, 2000.

Webb K.J., Black C.J.J. and H. Al-Jeel, Low Salinity oil recovery – log inject log, SPE 89379, 2004.

Webb K.J., Black C.J.J. and I.J. Edmonds, Low salinity oil recovery – the role of reservoir condition corefloods, EAGE conference, Budapest, Hungary, 2005.

Zhang Y. and N.R. Morrow, Waterflood performance by injection of brine with different salinity of reservoir cores, SPE 109849, 2007.